ISSN 2176-5480

22nd International Congress of Mechanical Engineering (COBEM 2013)
November 3-7, 2013, Ribeirão Preto, SP, Brazil

MODELING PSEUDOELASTIC VIBRATION ATTENUATORS ELEMENTS USING THE FINITE ELEMENT METHOD

Rodolpho Barbosa da Hora
Arthur Adeodato
Ivan Ivanovitsch Thesi Riagusoff
Ricardo Alexandre Amar de Aguiar
Pedro Manuel Calas Lopes Pacheco
CEFET/RJ – PPEMM - Programa de Pós-Graduação em Engenharia Mecânica e Tecnologia de Materiais
Department of Mechanical Engineering
20.271.110 – Rio de Janeiro – RJ - Brazil
rodolphodahora@gmail.com, adeodatoarthur@hotmail.com, ivanthesi@yahoo.com.br,
ricardoaamar@yahoo.com.br, calas@cefet-rj.br

Abstract. *Shape memory alloys (SMAs) present the capability to develop large forces and displacements with low power consumption. Due its special characteristics SMAs has been used in many different applications. Although there are several commercial devices that use SMA springs as actuators or vibration absorbers, modeling of this type of element is not well established. Pseudoelastic hysteresis loop observed in austenitic SMAs is associated to energy dissipation. Therefore, pseudoelastic SMA elements can be used as vibration attenuators. This work presents a nonlinear numerical model based on the Finite Element Method to study the behavior of SMA vibration attenuators elements. The model considers the presence of two phases (martensite and austenite) and large displacements, and is applied to study the pseudoelastic behavior of SMA absorber elements composed by cylindrical bars submitted to axial and torsional loadings. Several conditions are analyzed with the proposed models to assess the capability of the pseudoeleastic SMA elements to dissipate energy.*

Keywords: *Shape Memory Alloys, Pseudoelasticity, Modeling, Numerical Simulation, Finite Element Method*

1. INTRODUCTION

Shape memory alloys (SMAs) present complex thermomechanical behaviors related to different physical processes. The most common phenomena presented by this class of material are the pseudoelasticity, the shape memory effect, which may be one-way (SME) or two-way (TWSME), and the phase transformation due to temperature variation. Besides these phenomena, there are more complicated effects that have significant influence over its overall thermomechanical behavior – for instance: plastic behavior, tension-compression asymmetry, plastic-phase transformation coupling, transformation induced plasticity, thermomechanical coupling, among others (Tanaka, 1990, Savi *et al.*, 2002, Paiva *et al.*, 2005, Paiva and Savi, 2006). The remarkable properties of SMAs are attracting much technological interest, motivating different applications in several fields of sciences and engineering. Aerospace, biomedical, and robotics are some areas where SMAs have been applied (Birman, 1997; Denoyer *et al*., 2000, Webb *et al.*, 2000; Machado and Savi, 2003; Bundhoo *et al*., 2009, Hartl *et al*., 2010, 2010a, Spinella and Dragoni, 2010; Min An *et al.*, 2012).

Shape memory alloys (SMAs) have the capability to generate large strains associated to phase transformation induced by stress and/or temperature variations (Hodgson et al., 1992; Rogers, 1995). During the phase transformation process of a SMA component large loads and/or displacements can be generated in a relatively short period of time making this component an interesting mechanical actuator. Two phases are present: martensite and austenite (Zhang *et al.*, 1991). For lower temperatures, below a critical temperature, twined martensite phase is the only stable phase in a stress-free state, whereas detwined martensite is associated to the presence of a stress field above a critical stress. Several alloys can develop strains associated to phase transformation but only those that can develop large strains are of commercial interest, as nickel-titanium (NiTi) and copper base alloys (CuZnAl and CuAlNi).

Pseudoelastic effect occurs at higher temperatures, above a critical temperature (A_F) where austenite phase is the only stable phase in a stress-free state. Figure 1*a* presents a stress-strain curve (σ x ε) for the pseudoelastic effect at a constant temperature. In the loading process, a linear behavior (*OA)* is first observed followed by a nonlinear behavior (*AB*) associated to phase transformation (austenite → martensite). After point *B* the presence of 100 % of martensitic phase reveals a linear behavior. In the unloading process a linear behavior is observed until point C is reached. After that, a nonlinear behavior (*CD*) associated to phase transformation (martensite → austenite) is observed followed by a linear behavior associated to the presence of 100% of austenite. Figure 1*b* presents a diagram that illustrates the pseudoelastic behavior. A_S and A_F are the temperatures at which the formation of austenite starts and ends, respectively. M_S and M_F are the temperatures at which the formation of martensite starts and ends, respectively.

ISSN 2176-5480

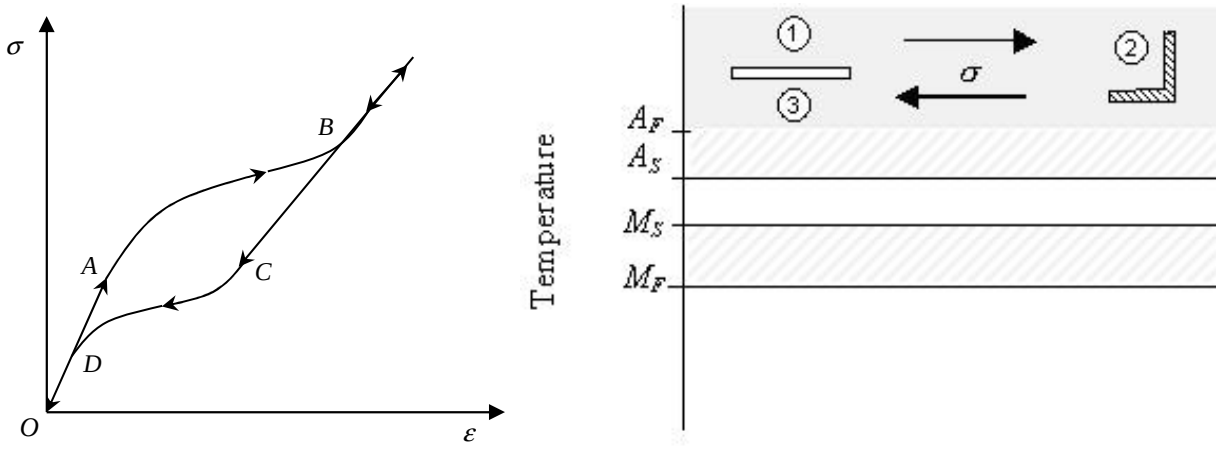

(*a*) (*b*)

Figure 1. Pseudoelastic effect. Stress-strain curve (*a*) and a diagram to illustrate the pseudoelastic effect (*b*) (Pereira, 2009).

Pseudoelastic effect observed in SMAs can be used to dissipate energy, making this material appropriate to be used in vibration attenuation applications (Aguiar *et al.*, 2013, Asgarian & Moradi,2011, Casciati and Faravelli, 2009, Desroches and Delemont, 2002, Fugazza, 2003, Johnson *et al.*, 2008, Lagoudas, 2008, Ozbulut *et al*., 2007, 2010, 2011, Ozbulut and Hurlebaus, 2011, Savi *et al.*, 2011, Shook *et al.*, 2008, Youssef *et al*., 2008, Zhang *et al*., 2008, Zuo *et al*., 2006, 2008, 2009, Zuo and Li, 2011). This effect is associated to hysteretic behavior that promotes mechanical energy dissipation during each cycle. Moreover, as austenite and martensite have different Young modulus values, during phase transformation the stiffness of an SMA element varies which affects the system dynamical behavior. Another remarkable feature of SMAs is its ability to change its center point (recentering) trough phase transformation induced by temperature or by a pre-loading (Pugliese and Casey, 2012). Due this combined effects, SMAs pseudoelastic elements are efficient vibration attenuation mechanical elements. Figure 2*a* shows a load-displacement curve for a SMA element subjected to an axial loading where the area inside the hysteresis loop represents the maximum energy dissipated during a loading-unloading cycle. Figure 2*b* shows a cyclic loading where oscillations occur between maximum and minimum load values (F_{max} and F_{min}). The energy dissipated in each cycle is associated to the highlighted area.

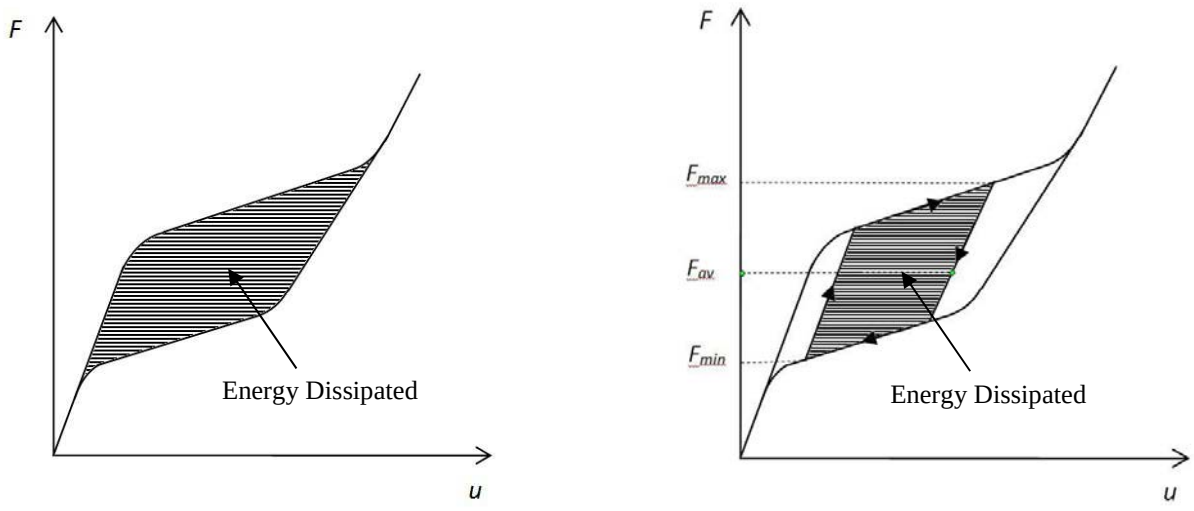

(*a*) (*b*)

Figure 2. Energy dissipation on pseudoelastic elements. (*a*) (*b*) dissipated energy for a vibration situation.

The availability of existing numerical tools coupled with advanced constitutive models has permitted advances in the modeling of the complex behaviors of SMAs material. In this work, numerical models based on finite element method were developed to evaluate the capability of passive SMA element vibration attenuators to dissipate energy.

ISSN 2176-5480

2. SHAPE MEMORY ALLOY CONSTITUTIVE MODEL

SMA thermomechanical behavior can be described by different constitutive models. Paiva & Savi (2006) presented an overview of constitutive models for SMAs. Here, the constitutive model proposed by Auricchio *et al.* (1997) is employed. This three-dimensional model is capable to describe the pseudoelastic behavior and considers the presence of two phases: austenite (*A*) and matrensite (*M*). The internal variables ξ_A and ξ_M are introduced to represent, respectively, austenitic and martensitic volume fractions that satisfies the following relation: $\xi_A + \xi_M = 1$. Material is considered isotropic and phase transformation obeys a Drucker-Prager loading function. Elastic behavior for austenite and martensite is related to the Young modulus (E) and Poisson ratio (ν). The process of phase transformation is controlled by 4 critical stresses σ_s^{AM}, σ_f^{AM}, σ_s^{MA}, σ_f^{MA}, where "*s*" and "*f*" subscripts states for "start" and "finish" and "*AM*" represents austenite to martensite transformation whereas "*MA*" represents martensite to austenite transformation. ε_L represents a parameter associate to recoverable strain resultant from martensitic phase transformation. Figure 3 presents an idealized one-dimensional stress-strain curve for the pseudoelastic behavior for the model used.

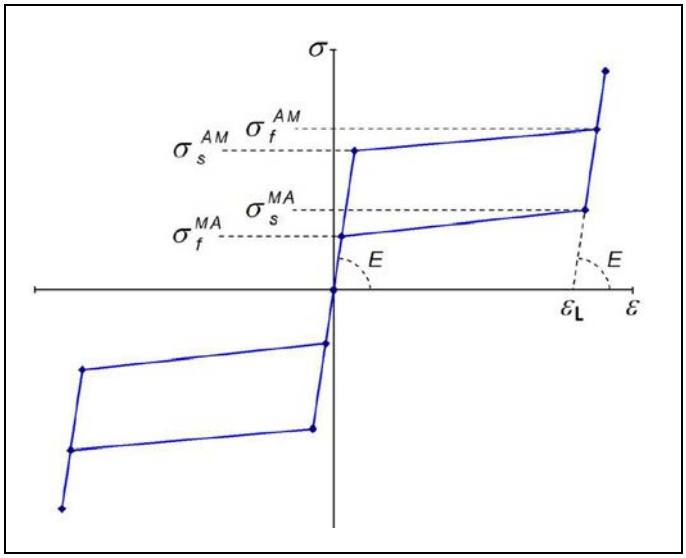

Figure 3. Idealized one-dimensional stress-strain curve for the pseudoelastic behavior. Auricchio *et al.* (1997) model.

3. FINITE ELEMENT MODEL

Tri-dimensional finite element models using the pseudoelastic constitutive model described in the last section were used to study the energy dissipation capability of SMA cylindrical bars submitted to axial and torsional loadings. Large displacements are considered in the analysis. The numerical simulations were performed with commercial finite element code ANSYS (Ansys, 2012), employing coupled thermal and mechanical fields element SOLID 186 for spatial discretization. This element is a tridimensional element with 20 nodes and the capability to describe pseudoelastic behavior through the incorporation of the Auricchio *et al.* (1997) constitutive model. The presented numerical simulations consider SMA mechanical components with the material properties represented in Table 1.

Table 1. SMA mechanical properties (Riagusoff, 2012).

Mechanical Properties	Value
E (GPa)	45
ν	0.30
σ_s^{AM} (MPa)	620
σ_f^{AM} (MPa)	750
σ_s^{MA} (MPa)	200
σ_f^{MA} (MPa)	100
ε_L	0.07

ISSN 2176-5480

Figures 4 and 5 present, respectively, the geometries and the meshes obtained after a convergence analysis, for the 4 SMA absorber elements analyzed: a cylindrical bar and three hollow cylindrical bars (internal to external radius ratio R_i /R_e = 0.25, 0.5 and 0.75) submitted to axial and torsional loadings. All the cylinders have an external diameter and length of 5 mm. For the axial loading, a pressure is applied at one end while prescribed zero displacements are applied at the other end in the loading direction. For the torsional loading, a torque is applied at one end while prescribed zero displacements is applied at the other end for all the degrees of freedom. Variables are analyzed at a central section to avoid the effects of the loadings and prescribed boundary conditions at the two cylinder ends.

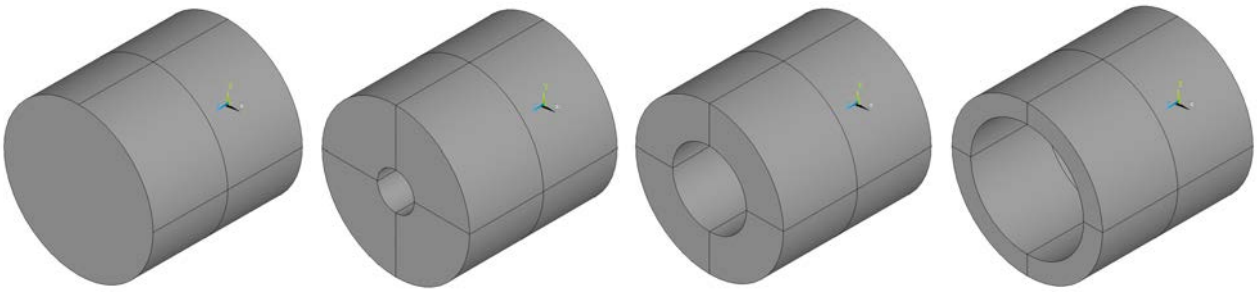

(*a*) (*b*) (*c*) (*d*)

Figure 4. Geometries analyzed: (*a*) cylindrical bar, (*b*) hollow cylindrical bar R_i / R_e = 0.25, (*c*) hollow cylindrical bar R_i / R_e = 0. 50, (*d*) hollow cylindrical bar R_i / R_e = 0.75.

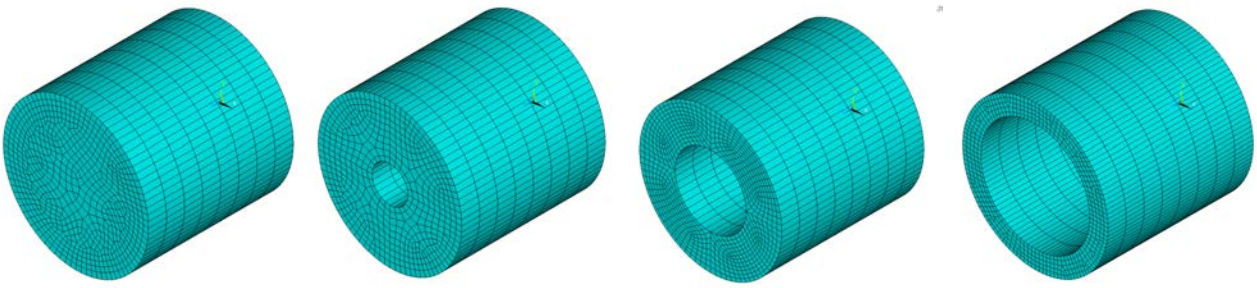

(*a*) (*b*) (*c*) (*d*)

Figure 5. Meshes for the geometries analyzed: (*a*) cylindrical bar, (*b*) hollow cylindrical bar R_i / R_e = 0.25, (*c*) hollow cylindrical bar R_i / R_e = 0. 50, (*d*) hollow cylindrical bar R_i / R_e = 0.75.

4. NUMERICAL RESULTS

To permit a direct comparison of the performance among the several geometries studied, all the bars are submitted to mechanical loadings (axial or torsional) that promote a maximum von Mises equivalent stress of 1.6 GPa. This value is considered a maximum allowable project stress before material experiments plastic strain.

Uniform bars submitted to axial loads are efficient absorber elements as they experiment homogeneous uniaxial stress state and therefore the whole bar experiments complete hysteresis loops cycles. This condition is associated to a maximum theoretical energy absorption density that can be estimated through the integration of the material pseudoelastic stress-strain hysteresis curve. Figure 6 presents the stress (σ) versus strain (ε) and load (F) versus displacement (u) curve obtained for a numerical simulation of the cylindrical bar submitted to axial loading. The material pseudoelastic stress-strain hysteresis curve furnishes an area equal to 39.2 J/m^3.

ISSN 2176-5480

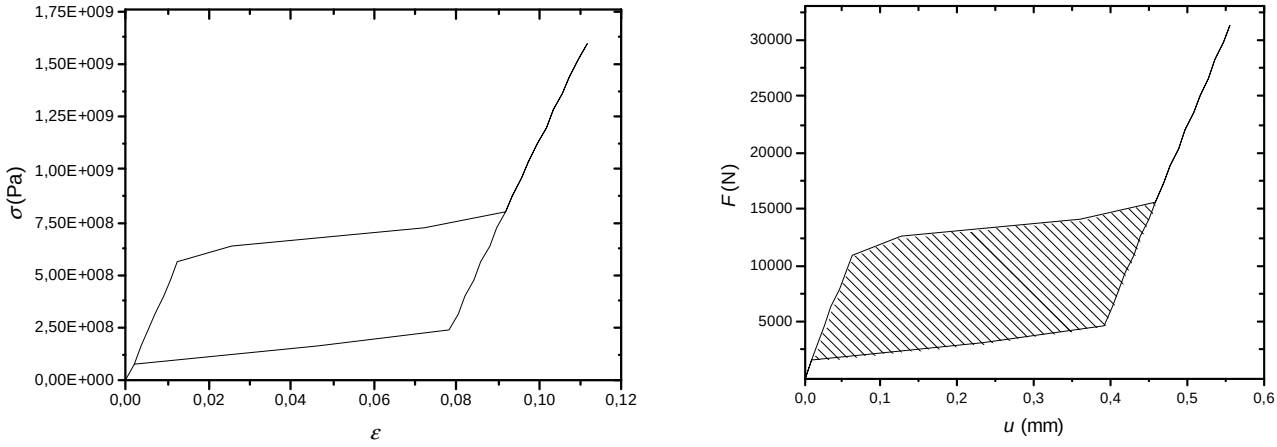

(*a*) (*b*)

Figure 6. Stress-strain curve (*a*) and load displacement curve (*b*) for axial loading.

Now the torsional load is considered for the 4 geometries described in Fig. 4. Figure 7 shows the von Mises equivalent stress distribution while Fig. 8 shows the martensitic volumetric phase distribution. Torsional load promotes a shear stress circumferential distribution with zero values at the center and maximum values at the surface. Therefore maximum values of von Mises equivalent stress and martensitic volumetric phase occurs at the cylinder surface.

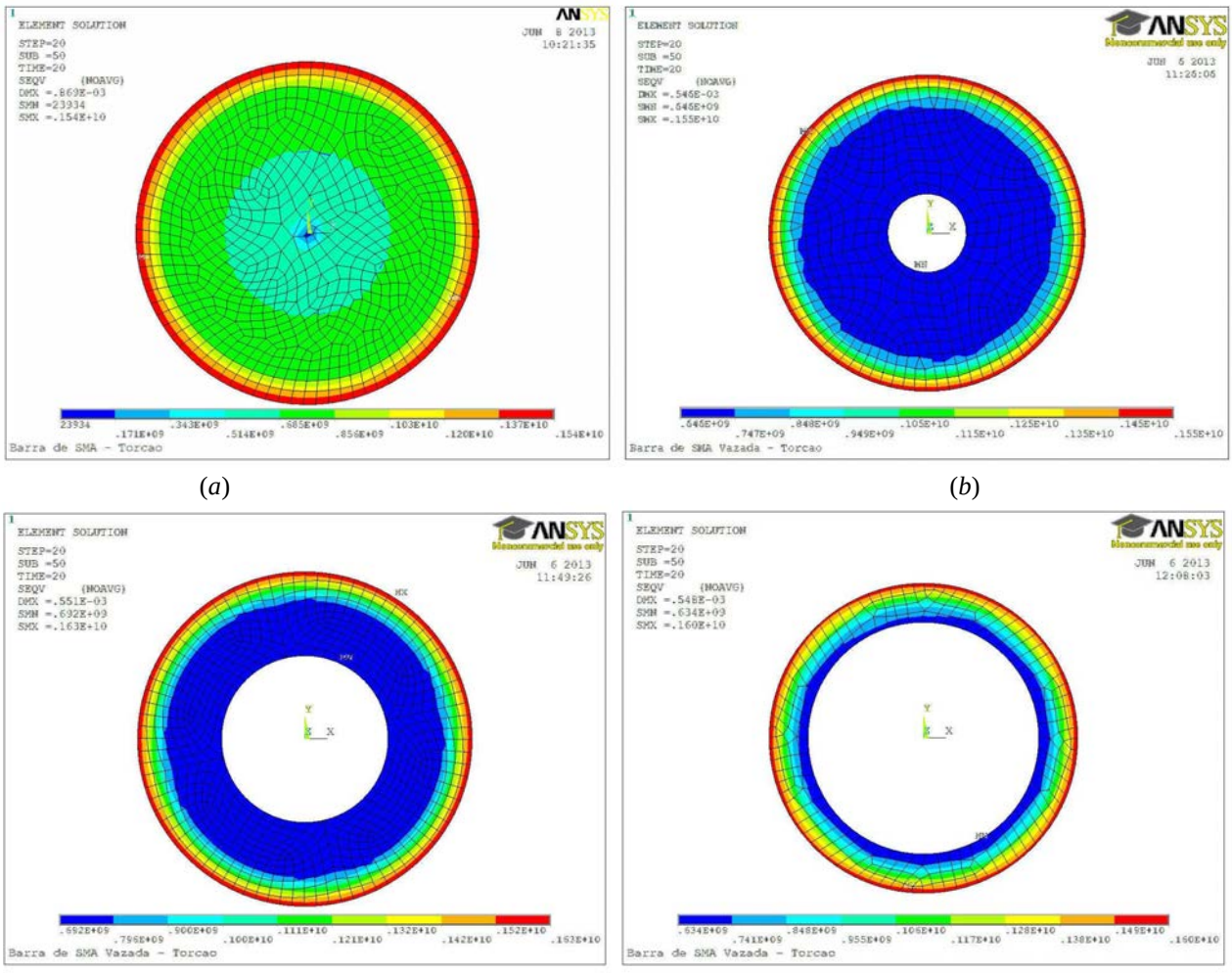

(*a*) (*b*)

(*c*) (*d*)

Figure 7. Von Mises equivalent stress distribution: (*a*) cylindrical bar, (*b*) hollow cylindrical bar R_i / R_e = 0.25, (*c*) hollow cylindrical bar R_i / R_e = 0. 50, (*d*) hollow cylindrical bar R_i / R_e = 0.75.

ISSN 2176-5480

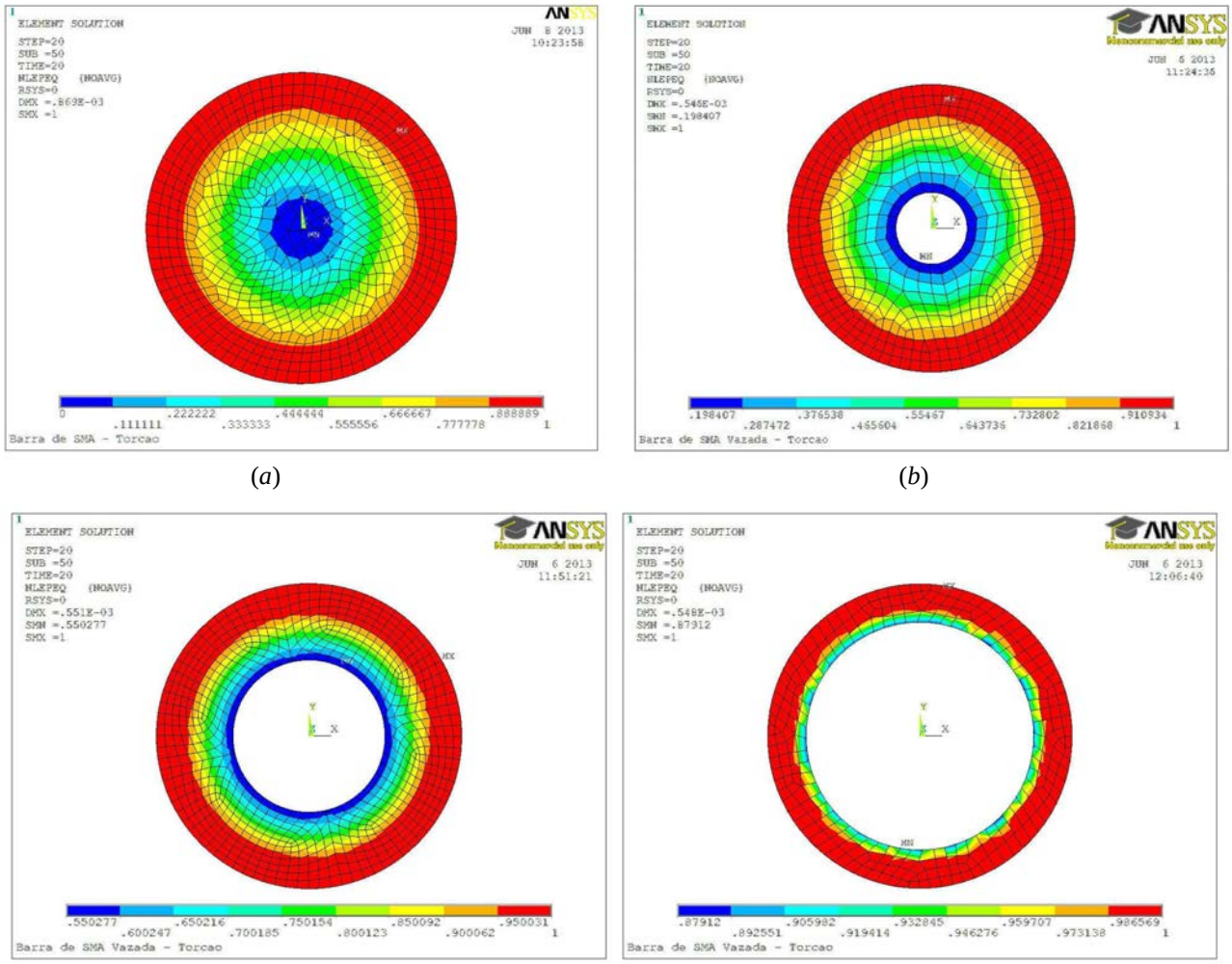

Figure 8. Martensitic volumetric phase distribution: (*a*) cylindrical bar, (*b*) hollow cylindrical bar R_i / R_e = 0.25, (*c*) hollow cylindrical bar R_i / R_e = 0. 50, (*d*) hollow cylindrical bar R_i / R_e = 0.75.

Figure 9 shows the cross section shear stress and martensitic volumetric phase distribution represented as a function of the cylinder radius (*r*) for all the 4 cylinders. As expected, results show that similar distributions are obtained and the central region of the cylinders experiment low stress and martensitic volumetric phase values. Therefore this region has a low contribution for energy dissipation. For cylinder with R_i / R_e = 0.75 almost all the cross section has martensitic volumetric phase values near 100% (between 87.9 and 100%).

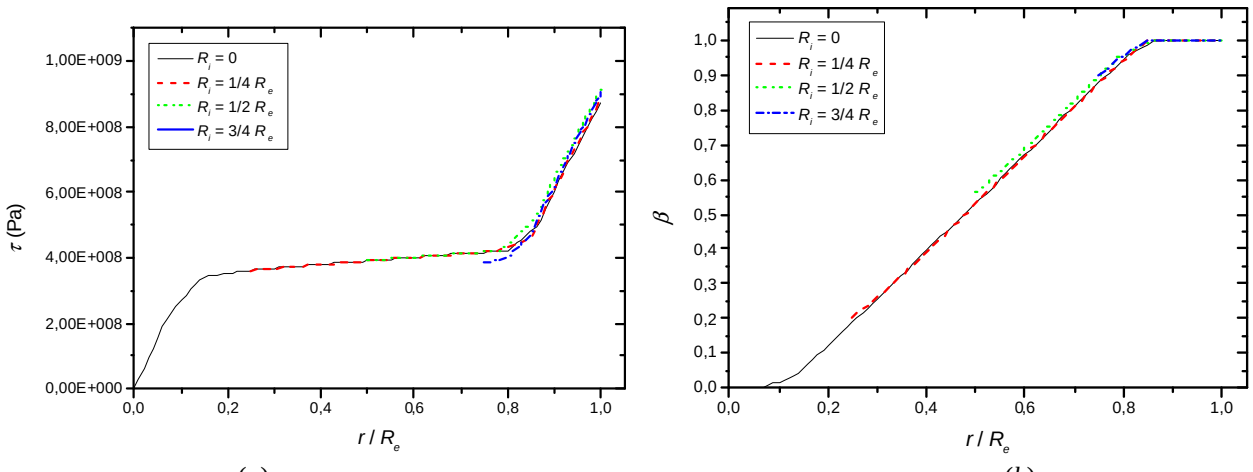

Figure 9. Shear stress distribution (*a*) and (*b*) Martensitic volumetric phase distribution at the cross section.

ISSN 2176-5480

Figure 10 presents the torque (T) versus angle (ϕ) curve for the 4 geometries of cylindrical bars submitted to torsional loading. The internal area associated to the hysteresis loop is highlighted. The applied torque decreases from 18 N.m to near 12 N.m and the hysteresis loop area also decreases, indicating that the dissipated energy decreases.

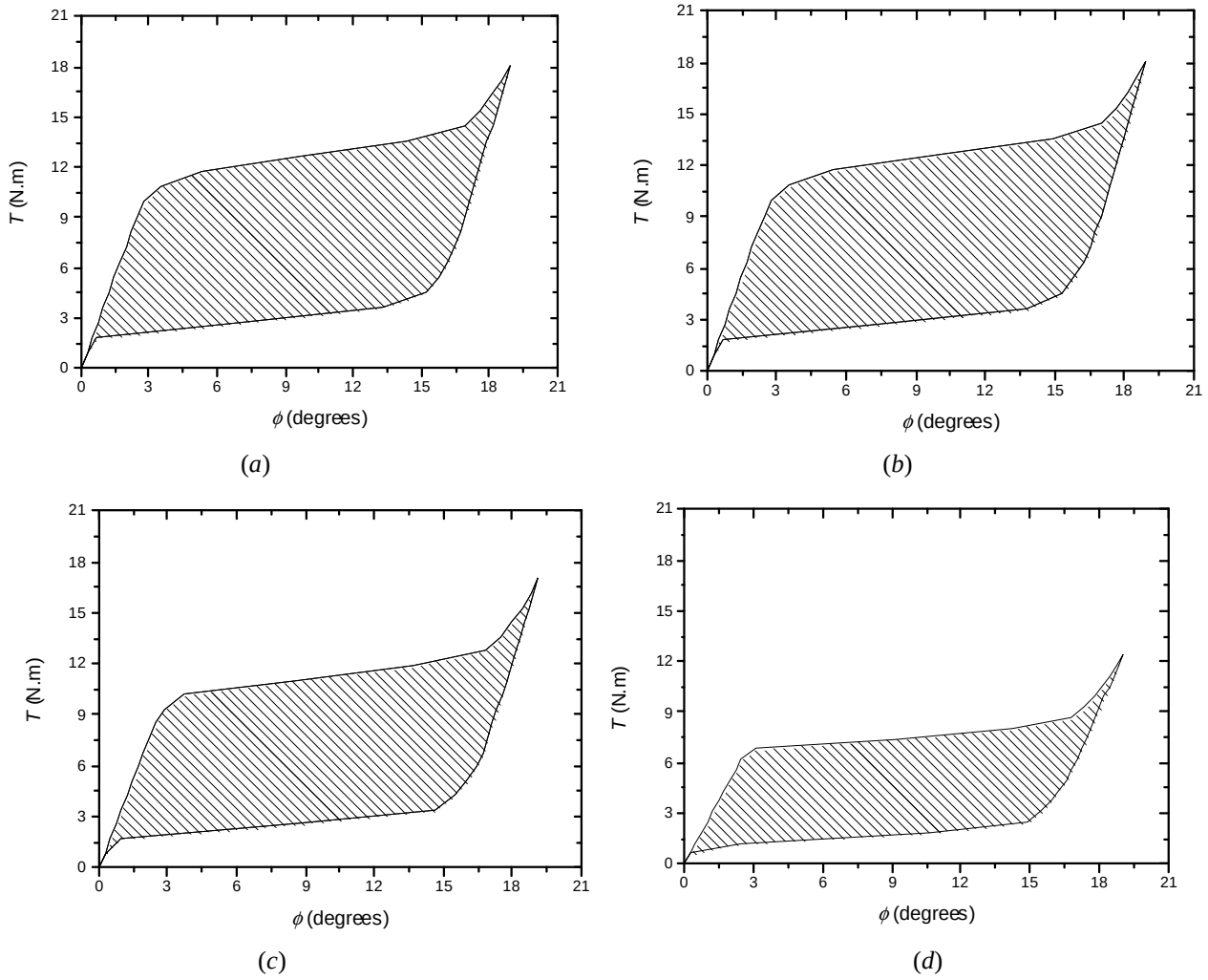

Figure 10. Torque versus angle curve: (*a*) cylindrical bar, (*b*) hollow cylindrical bar R_i / R_e = 0.25, (*c*) hollow cylindrical bar R_i / R_e = 0. 50, (*d*) hollow cylindrical bar R_i / R_e = 0.75.

Table 2 presents the energy dissipation, volume and energy dissipation density for the 4 cylinders. In Figure 11 the data associated to the 4 cylinders is normalized for the full cross section cylinder. Results shows that as the cylinder internal hole radius increases (from R_i/R_e = 0 to R_i/R_e = 0.75) energy dissipation decreases and volume decreases. However the energy dissipation density (energy/volume) increases, indicating that the hollow cylinders are efficient elements to absorb energy. From R_i/R_e = 0 to R_i/R_e = 0.75 is observed an energy dissipation decrease of 39.5 % and a volume reduction of 56.1%. The energy dissipation density increase is equal to 38.1%. Therefore the cylinder weight reduction is larger than the energy dissipation reduction.

Table 2. Energy dissipation, volume and energy dissipation density for the cylinders submitted to torsional load.

Cylinder Geometry (R_i/R_e)	Energy Dissipation (J)	Volume (mm^3)	Energy Dissipation Density (J/m^3)
0	144. 7	98.0	25.7
0.25	144.2	92.0	27.3
0.50	131.6	73.6	31.2
0.75	87.5	43.0	35.5

ISSN 2176-5480

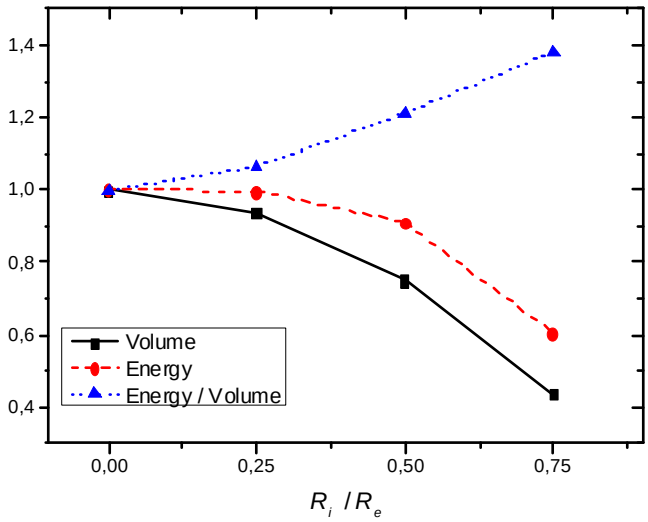

Figure 11. Normalized data for torsional loading of cylindrical bars.

Figure 12 presents a summary of the energy dissipation density for all the cases studied: cylinder submitted to axial load and the 4 cylinder geometries submitted to torsional load. Axial load results in the maximum energy dissipation density as all the cross section experiments a full phase transformation cycle. Cylinders submitted to torsional loads experiments maximum phase transformation at the surface and the centre presents a low contribution to energy dissipation as it experiments low values of phase transformations. The removal of this central region contributes to reduce the element weight and increases the energy dissipation density. Therefore hollow cylinders submitted to torsional loads are efficient energy dissipation elements.

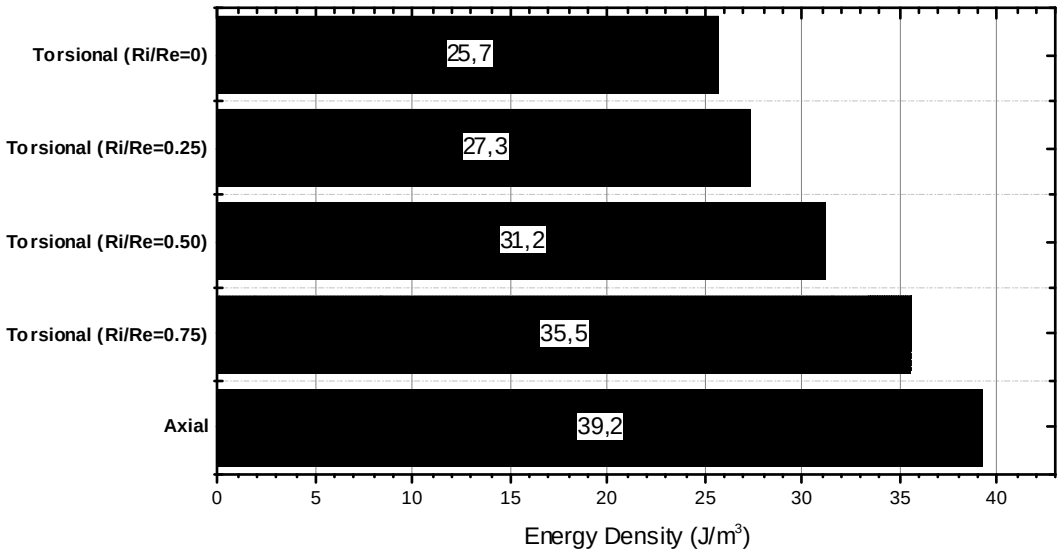

Figure 12. Energy dissipation density for the analyzed cases.

5. CONCLUSIONS

The pseudoelastic hysteresis loop observed in austenitic SMAs is associated to energy dissipation. Therefore pseudoelastic SMA elements can be used as vibration attenuators. In this work a nonlinear numerical model based on the Finite Element Method is proposed to study the capability of SMA elements to dissipate energy. The proposed model is applied to the study of cylindrical bars submitted to axial and torsional loadings. Full and hollow cross section cylinders are considered.

ISSN 2176-5480

Numerical results show that hollow cylinders can be used as efficient vibration absorber elements as they have large values of energy dissipation density. The proposed model can be used to study the performance of other geometries as helical or Belleville springs.

6. ACKNOWLEDGEMENTS

The authors would like to acknowledge the support of the Brazilian Research Agencies CNPq and CAPES.

7. REFERENCES

Aguiar, R.A.A., Savi, M. A. and Pacheco, P.M.C.L., 2013. “Experimental investigation of vibrationreduction using shape memory alloys”, *Journal of Intelligent Material Systems and Structures*, Vol. 24, p. 247-261.

ANSYS, 2012. “Structural Analysis Guide”, Release 14.

Asgarian, B. and Moradi, S., 2011. "Seismic Response of Steel Braced Frames with Shape Memory Alloy Braces", *Journal of Constructional Steel Research*, Vol. 67, p. 65-74.

Auricchio, F., Taylor, R.L. and Lubliner, J., 1997. ”Shape-Memory Alloys: Macromodeling and Numerical Simulations of the Superelastic Behavior”, *Computational Methods in Applied Mechanical Engineering*, Vol.146 , p.281-312.

Auricchio, F., 2001. “A Robust Integration-Algorithm for a Finite-Strain Shape-Memory-Alloy”, *International Journal of Plasticity*, Vol. 17, p.971-990.

Auricchio, F. and Stefanelli, U., 2004. Numerical analysis of a three-dimensional super-elastic constitutive model, *Journal for Numerical methods in engineering*, Vol. 61, p.142–155.

Auricchio, F. and Petrini, L., 2005. “Improvements and Algorithmical Considerations on a Recent Three-Dimensional Model Describing Stress-Induced Solid Phase Transformations”, *International Journal for Numerical Methods in Engineering*, Vol 55, p.1255-1284.

Bundhoo, V. Haslam, E., Birch, B.and Park, E. J., 2009. “A Shape Memory Alloy-Based Tendon-Driven Actuation System for Biomimetic Artificial Fingers, Part I: Design and Evaluation”, *Robótica*, Vol. 27, p. 131-146.

Casciati, F. and Faravelli, L., 2009. "A passive Control Device with SMA Components: from the Prototype to the Model", *Structural Control and Health Monitoring*, Vol. 16, p. 751–65.

Denoyer, K. K., Scott Erwin, R. and Ninneman, R., 2000, “Advanced smart structures flight experiments for precision spacecraft”, *Acta Astronautica*, Vol. 47, p.389-397.

Desroches, R. and Delemont, M., 2002, "Seismic Retrofit of Simply Supported Bridges Using Shape Memory Alloys", *Engineering Structures*, Vol. 24, pp. 325-332.

Johnson, R., Padgett, J. E., Maragakis, M. E., Desroches, R. and Saiidi, M. S., 2008. “Large scale testing of Nitinol shape-memory alloy devices for retrofitting of bridges", *Smart Materials and Structures*, Vol. 17, p. 1-10.

Fugazza, D., 2003. *Shape-Memory Alloy Devices in Earthquake Engineering: Mechanical Properties, Constitutive Modeling and Numerical Simulations*, Master degree thesis, Università degli Studi di Pavia.

Hartl, D. J., Lagoudas, D. C., Calkins, F. T. and Mabe, J. H., 2010. "Use of a Ni60Ti Shape Memory Alloy for Active Jet Engine Chevron Application: I. Thermomechanical Characterization", *Smart Materials and Structures*, Vol. 19, n. 20, p. 1-14.

Hartl, D. J., Lagoudas, D. C., Calkins, F. T., Mabe, J. H., 2010a. "Use of a Ni60Ti Shape Memory Alloy for Active Jet Engine Chevron Application: II. Experimentally Validated Numerical Analysis", *Smart Materials and Structures*, Vol. 19, n. 21, p. 1-18

Hodgson, D. E., Wu, M. H. and Biermann, R. J., 1992. “Shape Memory Alloys”, ASM Handbook, Vol. 2, p. 887-902.

Lagoudas, D.C., 2008. *Shape Memory Alloys - Modeling and Engineering Applications*, Springer.

Machado, L.G. and Savi, M.A., 2003. “Medical applications of shape memory alloys, *Brazilian Journal of Medical and Biological Research*, Vol. 36, p. 683-691.

Min An, S., Ryu, J., Cho, M. and Cho, K.J., 2012. “Engineering design framework for a shape memory alloy coil spring actuator using a static two-state model”, *Smart Materials and Structures*, Vol. 21, p.1-16.

Ozbulut, O. E., Mir, C., Moroni, M. O., Sarrazin, M. and Roschke, P. N., 2007. "A Fuzzy Model of Superelastic Shape Memory Alloys for Vibration Control in Civil Engineering Applications", *Smart Materials and Structures*, Vol. 16, p. 818-829.

Ozbulut, O. E., Roschke, P. N., Lin, P. Y. and Loh, C. H., 2010. "GA Based Optimum Design of a Shape Memory Alloy Device for Seismic Response Mitigation", *Smart Materials and Structures*, Vol. 19, p. 1-14.

Paiva, A., Savi, M.A., Braga, A. M. and Pacheco, P.M.C.L., 2005. “A constitutive model for shape memory alloys considering tensile-compressive asymmetry and plasticity”, *International Journal of Solids and Structures*, Vol. 42, p.3439-3457.

Paiva, A. and Savi, M. A., 2006. “An Overview of Constitutive Models for Shape Memory Alloys”, *Mathematical Problems in Engineering*, Vol. 2006, p. 1-30.

Pereira, J.H.I., 2009. *Um Estudo Sobre Atuadores Lineares com Molas Helicoidais de Ligas com Memória de Forma*, M.Sc. Thesis, CEFET/RJ – Prog. de Pós-Graduação em Tecnologia, Rio de Janeiro.

Pugliese, G. and Casey, D., 2012. “Analysis of Shape Memory Alloy and Their Application for Reducing Damage Due to Seismic Activity”, University of Pittsburgh - Swanson School of Engineering.

Riagusoff, I. I. T., 2012. *Estudo de Dispositivos Pseudoelásticos para Aplicação em Atenuadores de Vibração*, M.Sc. Thesis, CEFET/RJ – Prog. Pós-Graduação em Eng. Mecânica e Tecnologia de Materiais, Rio de janeiro.

Rogers, C.A., 1995. Intelligent Materials, *Scientific American*, September, p.122-127.

Savi, M.A., Paiva, A., Baêta-Neves, A.P. and Pacheco, P.M.C.L., 2002. “Phenomenological modeling and numerical simulation of shape memory alloys: A thermo-plastic-phase transformation coupled model”, *Journal of Intelligent Material Systems and Structures*, Vol. 13, p.261-273.

Savi, M.A., De Paula, A.S. and Lagoudas, D.C., 2011. “Numerical investigation of an adaptive vibration absorber using shape memory alloys”, *Journal of Intelligent Material Systems and Structures*, Vol. 22, p. 67-80.

Shook, D., Lin, P. Y., Lin, T. K. and Roschke, P. N., 2007. "A Comparative Study in the Semi-active Control of Isolated Structures", *Smart Materials and Structures*, Vol. 16, p. 1433-1446.

Spinella, I. and Dragoni, E., 2010. “Analysis and Design of Hollow Helical Springs for Shape Memory Actuators”, *Journal of Intelligent Material Systems and Structures*, Vol. 21, p.185-199.

Tanaka, K., 1990. “A Phenomenological Description on Thermomechanical Behavior of Shape Memory Alloys”, *Journal of Pressure Vessel Technology*, 112, p.158-163.

Webb, G., Wilson, L., Lagoudas, D.C. and Rediniotis, D.C., 2000. “Adaptive Control of Shape Memory Alloy Actuators for Underwater Biomimetic Applications”, *IAAA Journal*, Vol. 38, p.325-334.

Zhang, X.D., Rogers, C.A. & Liang, C., 1991, “Modeling of Two-Way Shape Memory Effect”, *ASME - Smart Structures and Materials*, Vol. 24, p.79-90.

Zhang, Y., Camilleri, J.A. and Zhu, S., 2008. ‘‘Mechanical Properties of Superelastic Cu-Al-Be Wires at Cold Temperatures for Seismic Protection of Bridges,’’ *Smart Materials and Structures*, Vol. 17, p. 1-9.

Zuo, X. B., Chang, W., Li, A. Q. and Chen, Q. F., 2006. "Design and Experimental Investigation of a Superelastic SMA Damper", *Materials Science and Engineering A*, Vol. 438-440, p. 1150-1153.

Zuo, X. B., Li, A. Q., Chen and Q. F., 2008. "Design and Analysis of a Superelastic SMA Damper", *Journal of Intelligent Material Systems and Structures*, Vol. 19, p. 631-639.

Zuo, X., Li, A., Sun, W. and Sun, X., 2009. "Optimal Design of Shape Memory Alloy Damper for Cable Vibration Control", *Journal of Vibration and Control*, Vol. 15, p. 897-921

Zuo, X. and Li, A., 2011. “Numerical and Experimental Investigation on Cable Vibration Mitigation Using Shape Memory Alloy Damper”, *Structural Control Health and Monitoring*, Vol. 18, p. 20-39.

8. RESPONSIBILITY NOTICE

The authors are the only responsible for the printed material included in this paper.